FUNCTIONALIZED ZnO/CdS COMPOSITES: SYNTHESIS, CHARACTERIZATION AND PHOTOCATALYTIC APPLICATIONS

A. DUMBRAVA[a,*], D. BERGER[b], G. PRODAN[c], F. MOSCALU[d]
[a]*Department of Chemistry and Chemical Engineering, Ovidius University of Constanta, Romania*
[b]*Department of Inorganic Chemistry, Physical Chemistry and Electrochemistry, University Politehnica of Bucharest, Romania*
[c]*Electron Microscopy Laboratory, Ovidius University of Constanta, Romania*
[d]*Department of Physics, Ovidius University of Constanta, Romania*

We synthesized ZnO/CdS composites using two strategies for the deposition of functionalized/capped CdS nanoparticles onto ZnO surface. The structure and morphology of the obtained materials were investigated by X-ray diffraction and transmission electron microscopy. The optical properties were studied using UV-Visible diffused reflectance spectroscopy and the catalytic activity was explored in the photodegradation of Congo red azo dye. The optical properties and the photocatalytic activity were compared with those of functionalized/capped CdS nanopowders obtained in the same conditions, and the results revealed broader absorption bands, together with higher energy gaps, and also the improvement of photocatalytic properties.

1. Introduction

　　　　Cadmium sulfide and zinc oxide are both very important semiconductors, having applications in various domains like: energy conversion [1], electronic devices [2], catalysis [3], etc. Cadmium sulfide, as bare and/or functionalized powder or thin film, was remarked as a versatile and efficient material [4, 5], its properties varying with the particles morphology [6]. However, despite its very convenient optical properties, which make CdS a significant semiconductor and a good photocatalyst, cadmium compounds may be toxic and a low content of CdS in a catalyst system is desired. On the other hand, the more environmental friendly zinc oxide cannot absorb the visible region of the solar spectrum (>420 nm) and an inventive solution was to couple the zinc oxide to a narrower band gap sensitizing semiconductor in composite materials which absorb the visible light, generate the electron–hole pairs and exhibit an effective photocatalytic activity [1]. The composite materials are designed in order to tune the optical properties and to enhance the semiconductor structures functionality for device applications, having superior features compared to the individual components [7]. These materials exhibit advantages because they can compensate the individual component drawbacks, and induce a synergistic effect, such as an efficient charge separation and enhanced photostability [8]. New properties and various functionalities have been achieved by assembling different components into composites by tuning the structure and interface interactions [9]. In this trend, we associated in the present study the cadmium sulfide, a semiconductor which presents a band gap in the visible region ($E_g \approx 2.4$ eV at 300 K) [10] with zinc oxide, a semiconductor with a wide band gap ($E_g \approx 3.3$ eV at 300 K) corresponding to emission in the UV region [2]. The ZnO-based semiconductor composites are very interesting materials because of possible synergistic effects on

---

*Corresponding author: adumbrava@univ-ovidius.ro

photoelectrochemical properties and photocatalytic activity [11, 12]. Hence, it is known that ZnO acts as a catalyst under ultraviolet excitation and could also exhibit activity under visible excitation if it is coupled with another semiconductor (CdS or CdSe); in a composite like ZnO/CdS, CdS acts as a visible sensitizer and ZnO is responsible for charge separation suppressing the recombination process [7]. CdS is the most suitable visible sensitizer for ZnO because its lattice is similar with ZnO, having the band gap in the visible range and forming a type-II heterojunction with ZnO, which facilitates a very fast interband charge transfer from these two compounds [13]. The charge injection from one semiconductor to another leads to an efficient charge separation due to reduction in the exciton recombination; one of the excitons is confined to the core and the other to the shell [14]. The ZnO/CdS heterostructures with enhanced photocatalytic hydrogen generation have been developed via a direct *Z*-scheme mechanism, where the recombination of photoexcited electrons from the ZnO conduction band and holes from the CdS valence band occurs at the interface [15]. The ZnO/CdS coupling unit is widely used in *p-n* junction solar cells due to its excellent carrier transport at the interface [16].

The ZnO/CdS core–shell nanoparticles can also be used in environmental remediation (*e.g.* the degradation of orange-II, rhodamine B, eriochrome black T [17, 18]), as sensors [19], in solar cells [20], photocatalytic hydrogen generation [15, 21], etc. The sensitization of wide band gap semiconductors as ZnO and TiO_2 with CdS nanoparticles is also important for the quantum dots sensitized solar cells [22]. The synthesis methods for ZnO/CdS composites, as thermal decomposition of cadmium compounds on the surface of ZnO [14], chemical bath deposition on ZnO nanorods deposited on transparent conductive oxide glass [18], chemical precipitation [16, 17], pulsed laser deposition of CdS on hydrothermally grown ZnO nanorods [23], simple ultrasound-assisted solution phase conversion process using monodispersed ZnO nanospheres as a starting reactant and *in situ* template [24], etc. were reported in last years. The deposition of CdS nanoparticles can be performed in the ZnO synthesis medium (one-pot) [25, 26] or follows the synthesis of zinc oxide in a second step [14, 18]. Despite an important number of studies dealt with the synthesis of ZnO/CdS composites, the deposition of functionalized CdS nanoparticles onto ZnO surface was not considered enough; thus, in our knowledge, the mercaptoacetate-functionalized CdS nanoparticles were not previously used for the decoration of zinc oxide.

In our previous work, we obtained capped/functionalized CdS nanopowders, with high photocatalytic activity, by choosing the suitable techniques [27, 28]. In continuation of our study, we increased the photocatalytic activity of capped/functionalized CdS nanopowders with inferior performances, obtained in the same systems. Therefore, we studied the deposition of functionalized/capped CdS nanoparticles obtained by one-pot synthesis, as we previously reported, onto ZnO surface, in mild conditions, at room temperature. The properties of obtained composite materials were compared with those of CdS nanopowders prepared in similar conditions.

2. Experimental

2.1. Materials and methods
All the reagents were purchased from commercial sources and used as received.

The high purity reagents were obtained commercially from Sigma-Aldrich (cadmium acetate, $Cd(CH_3COO)_2 \cdot 2H_2O$; polyethylene glycol 200, PEG-200; sodium thioglycolate (sodium mercaptoacetate), $C_2H_3O_2SNa$; Congo red), Merck (thioacetamide, TAA), Loba Chemie (ZnO), and were used as received without further purification. The Congo red (CR, C.I. Direct Red 28, M.W. = 696.67 g mol^{-1}, $C_{32}H_{24}N_6O_6S_2Na_2$) is the disodium salt of 3, 3'-([1, 1'-biphenyl] - 4, 4' - diyl)bis(4 – aminonaphthalene - 1 - sulfonic acid).

2.2. Preparation of ZnO/CdS powders
ZnO/CdS **1**. ZnO (3.24 g, 40 mmol) and PEG-200 (2.5 mL) were mixed with 100 mL of water and magnetic stirred for 30 min. $Cd(CH_3COO)_2 \cdot 2H_2O$ (1.33 g, 5 mmol) and TAA (0.375 g, 5 mmol) were added in the resulted mixture. A yellow solid started to form instantly, indicating the synthesis of CdS. The mixture was stirred for 4 hours. The yellow powder was isolated by vacuum

filtration, washed with water and dried. Selected FT-IR data (KBr, cm^{-1}): 3376 (w), 1558 (w), 1508 (w), 1394 (w), 1090 cm^{-1} (vw), 1015 cm^{-1} (vw), 831 (vw), 496 (vs), 447 (vs), 414 (s).

ZnO/CdS **2**. Cd(CH$_3$COO)$_2$·2H$_2$O (1.33 g, 5 mmol) was dissolved in 1 mL PEG-200 using the trituration technique. TAA (0.375 g, 5 mmol) was added and the mixture was triturated, without adding water, until the complete dissolution of the reagents and a colorless paste was formed. In this paste, sodium mercaptoacetate (0.57 g, 5 mmol), ZnO (3.24 g) and an additional amount of PEG-200 (1.5 mL) were added. The resulted mixture was intermittently triturated and left overnight, and the mixture color turns in yellow – reddish. For the removal of the unreacted compounds and byproducts, the product was mixed with water (100 mL), stirred for 30 min and the yellow powder was isolated by vacuum filtration, washed with water and dried. Selected FT-IR data (KBr, cm^{-1}): 3385 (m), 1558 (m), 1375 (m), 1125 (w), 1075 (vw), 773(vw), 696 (vw), 497 (vs), 443 (vs), 415 (s).

2.3. Characterization of ZnO/CdS powders

The obtained powders were investigated by X-ray diffraction (XRD) performed on a Rigaku Miniflex 2 diffractometer with Ni filtered CuKα radiation, in the range of 2θ, 10-70°, scan rate of 2°/min and a step of 0.02°. The TEM investigations of ZnO/CdS powders were performed on a Philips CM 120 ST transmission electron microscope operated at 100 kV, with 2 Å resolution. The UV-VIS diffused reflectance spectra were recorded in the range 220 – 850 nm, on a Jasco V 550 spectrophotometer, in an integrating sphere. The IR spectra were recorded with Jasco FT-IR 4200 spectrometer from KBr pellets, in the range 400 – 4000 cm^{-1}.

2.4. Catalytic properties of ZnO/CdS powders

The photocatalytic degradation of CR was performed using for each determination 100 mL of 30 mg/L CR solution and 0.05 g ZnO/CdS as catalyst. Before irradiation, the dye solutions were stirred in the dark for 10 min after the addition of the catalyst, to reach the adsorption–desorption equilibrium.

The experiment was conducted in the same time with two samples, which were exposed to the ambient light, respective to a 20 W halogen lamp (Ecolite, China) as simulated visible light source. The spectrum of the lamp was measured with a HR4000CG-UV-NIR High-Resolution Spectrometer, from Ocean Optics, confirming the matching with the solar spectrum. The experiments were performed in covered Pyrex vessels of 250 mL capacity. The halogen lamp was irradiated perpendicularly to the surface of solution, and the distance between the UV-Vis source and vessel containing reaction mixture was fixed at 15 cm. The suspension was agitated with magnetic stirrer to get ensured that all the active sites of catalysts are in contact with the dye solution and exposed to light.

The suspension was sampled at regular intervals and immediately centrifuged at 5000 rpm for 10 min with a M 815 M centrifuge (from Elektro-Mag), and then filtered, to completely remove the catalyst particles. The degradation efficiency of CR was monitored by UV–Vis spectroscopy, using a Jasco FT-IR 4200 spectrometer.

The degradation of the dye was estimated by C_t/C_0 ratio, where C_t and C_0 are the concentrations of CR when the reaction time is t and 0, respectively. The catalyst efficiency may be also estimated by the degradation efficiency (R) or by the photocatalytic activity (PA) [29, 30], which can be calculated as [31]:

$$PA = \frac{C_0 - C_t}{C_0} x100 = \frac{A_0 - A_t}{A_0} x100$$

where A_0, A_t are the absorbance values for CR solution when the reaction time is 0 and t, respectively (on the basis of Lambert – Beer law).

The UV-VIS absorption spectra of CR solutions were recorded in the range 200 – 900 nm, on a Jasco V 550 spectrophotometer. The absorption peaks corresponding to CR were reported at 497 nm, 347 nm and 237 nm [32].

3. Results and discussion

We synthesized ZnO/CdS powders by the depositing of capped/functionalized CdS nanoparticles onto the ZnO surface, using two experimental techniques, namely the chemical precipitation in an aqueous solution and the trituration of a non-aqueous mixture. As we previously reported [27], the trituration of a non-aqueous mixture is a facile and really convenient method for synthesis of capped CdS nanoparticles with very high catalytic activity.

The obtained ZnO/CdS powders were characterized by XRD, TEM, FTIR and UV-Vis diffuse reflectance spectroscopy. The band gap energy was calculated by Tauc equation and the catalytic properties were determined in the Congo red photodegradation.

It has been accepted that the synthesis of metal sulfide colloidal nanoparticles typically consists in a chemical reaction between a metal salt and a sulfide ion precursor, in the presence of capping agents, in order to stabilize the high energy surface of the nanoparticles and protect them from aggregation [33]. Thus, the synthesis of CdS nanoparticles was carried out in the presence of a capping agent (PEG-200); the ZnO powder was added in the synthesis medium of CdS, obtained as we previously reported [27, 28] and, in consequence, the functionalized CdS nanoparticles were deposited onto the ZnO surface.

3.1. Characterization of ZnO/CdS powders
3.1.1. X-ray diffraction
The X-ray diffraction was used to identify the crystalline phases. The XRD patterns of both samples exhibited the Bragg reflections of ZnO phase with hexagonal symmetry, besides CdS peaks belonging to a mixture of cubic and hexagonal phases (less crystalline CdS was obtained in the case of ZnO/CdS **2** sample), which are shifted to lower values of 2θ (Fig. 1). This observation could be explained by a diffusion of zinc ions into the crystalline lattice of CdS at interface, in agreement with Estévez-Hernández *et al*. that claimed the formation of amorphous $Cd_{1-x}Zn_xS$ solid solution at the interface consisting in ZnS layer and the capping molecule, namely mercaptopropionic acid, in CdS/ZnS nanocomposites [34].
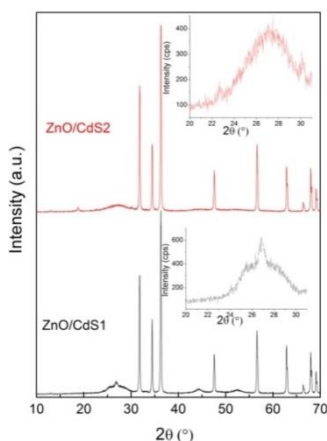
Fig 1. The XRD patterns of ZnO/CdS powders.

Also, Abe *et al*. investigated the ZnO/CdS interface by the XPS, XAFS and XANES measurements and they reported the formation of $CdSO_4$ at the ZnO/CdS interface, this compound being present on the CdS surface before the ZnO deposition [35].

3.1.2. Transmission electron microscopy

The ZnO/CdS powders morphology was furthermore investigated by TEM technique. The TEM images (Fig. 2) evidenced different shapes of ZnO particles, almost being nanorods with length in microns range and nanosized width, and the formation of CdS small particles (nanoparticles) on ZnO surface in ZnO/CdS powders.

Figure 2.a shows that, in ZnO/CdS **1,** the oxide particles are uniformly covered with CdS nanoparticles from bottom to top, forming ZnO/CdS core/shell composites. The CdS covered ZnO particles exhibit increased diameters and rough surfaces compared with the bare ZnO particles. Similar results were reported for ZnO/CdS nanocomposites obtained through other synthesis routes [23].

a)

b)
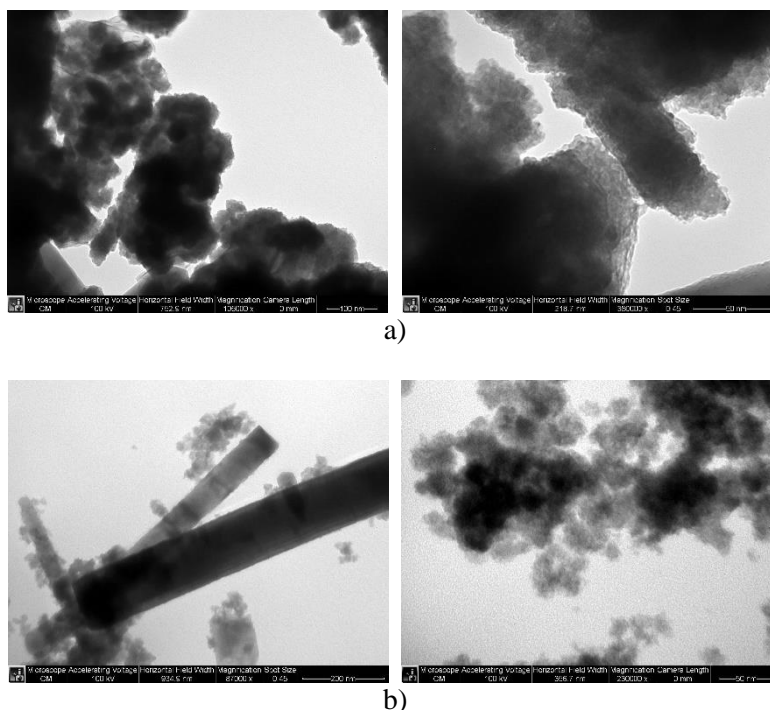
*Fig. 2. The TEM images for ZnO/CdS **1** (a) and ZnO/CdS **2** (b).*

On the contrary, for ZnO/CdS **2** (Fig. 2.b) the CdS nanoparticles formed only small aggregates, which are not very adherent to the surface of ZnO particles; in consequence, ZnO particles are not uniformly covered with CdS nanoparticles. In the case of ZnO/CdS **2** sample, the interface formed between CdS layer and the capping molecule (MAA) appears to be amorphous. This observation is also noticed for other particles capped with mercaptocarboxilate ions [28, 34]. This may be an explanation for the low adherence of CdS particles to ZnO.

3.1.3. FT-IR spectroscopy

The FTIR spectra of the synthesized ZnO/CdS composites were recorded for the identification of the functionalization/capping agents.

In both samples, the broad absorption bands demonstrated the presence of water molecules (ν_{OH}: 3376 cm^{-1} and 3385 cm^{-1} for ZnO/CdS **1** and ZnO/CdS **2**, respectively). The strong bands around 500 cm^{-1}, 450 cm^{-1} and 400 cm^{-1} are assigned to wurtzite ZnO phase [36]. In the FTIR spectrum of commercial ZnO from Loba Chemie, we identified two distinct bands located at 417 and 505 cm^{-1}, and a shoulder at about 515 cm^{-1} [37]. It was demonstrated [36, 38, 39] that the FTIR spectrum of ZnO particles might vary from a broad single band over the doublet up to a three-band superposition. This effect may be explained as a consequence of the geometrical shape of ZnO particles. The modification of the vibrations assigned to ZnO after the decoration with CdS nanoparticles may be correlated with a change of morphology, which is simultaneously with CdS

depositing on the surface. Besides the chemical composition and crystal structure, additional three factors, which influence the infrared vibrations of a material, are: (*i*) the dielectric constant of the matrix, in which material is diluted, (*ii*) the particles aggregation and (*iii*) the shape [38, 39]. Most probably, the FTIR spectrum of the initial ZnO powder was changed as a consequence of the interaction with PEG, which modified the morphology (*i.e.* the particles aggregation and shape) of pristine ZnO powder.

The other bands could be attributed to acetate (ν_{as}(COO): 1558 and 1508 cm^{-1}, ν_s(COO): 1394 cm^{-1} for ZnO/CdS **1**) and mercaptoacetate (ν_{as}(COO): 1558 cm^{-1}; ν_s(COO): 1375 cm^{-1} for ZnO/CdS **2**), which probable capped/functionalized the ZnO/CdS particles [40]. The presence of residual acetate in metal sulfides powder was reported previously by other authors [41]. The vibration band assigned to carboxylate group in sodium mercaptoacetate (1600 cm^{-1}) is splitted and shifted to lower wave numbers, the asymmetric and symmetric vibrations indicating the coordination of mercaptoacetate ion to cadmium atoms through the carboxylate group, similar with the results obtained by other authors for mercaptoacetate as capping/functionalizing agent [40, 42, 43].

For aliphatic ethers (like PEG) the C–O–C stretching bands are the most characteristic: a stronger band due to asymmetrical stretching at 1150-1085 cm^{-1} and a weaker band due to symmetrical stretching at lower wavelength [44]. Thus, the presence of PEG may be correlated with 1090 cm^{-1} and 1015 cm^{-1} vibrations (ZnO/CdS **1**), respective 1125 cm^{-1} and 1075 cm^{-1} vibrations (ZnO/CdS **2**). The low intensity of the bands assigned to PEG is due to the partial removal of capping agent by solvent washing, the removing being important for the catalytic properties because the capping agents can act as a physical barrier to restrict the free access of reagent to catalytically active sites on the particle surface [45].

3.1.4. UV-Vis spectroscopy

The optical properties of the ZnO/CdS powders were studied by the UV-Visible diffuse reflectance spectroscopy. The UV-Vis absorption spectra are shown in Fig. 3.
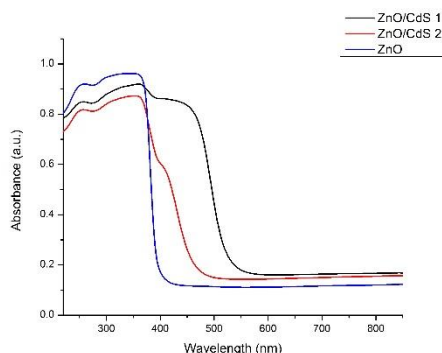
Fig. 3. The UV–Vis absorption spectra of ZnO/CdS powders in comparison with pristine ZnO powder.

As one can see in Fig. 3, the absorption bands of ZnO/CdS samples are broader compared with pristine ZnO, making the CdS-decorated zinc oxide materials more effective in many applications, as in heterogeneous catalysis or in solar cells. The bands assigned to CdS nanoparticles are slightly modified compared to the CdS nanopowders obtained in the same conditions [27, 28], which could mean a modification in the structure of band gap due to the interaction with ZnO and/or a modification of the CdS nanoparticles morphology, having in view the relation between the electronic spectrum and the morphology of powders. The shift may be also due to the formation of a solid solution at the core-shell interface, as the XRD suggested.

The intensity of absorption band at 400 nm is lower for ZnO/CdS **2** in comparison with ZnO/CdS **1**, which may be explained by a smaller quantity of CdS in ZnO/CdS **2**. This result is consistent with the TEM images, which show that CdS nanoparticles did not cover well the surface

of ZnO particles. For both samples the bands assigned to CdS are blue-shifted compared with the absorption edge of bulk cubic CdS (515 nm) [46].

3.1.5. Band gap energies

The band gap of semiconductor materials strongly influences their electrical and optical properties, so it is important to study their band gap changes for a better understanding of the relevant properties of this kind of materials. In many applications of ZnO and CdS (*e.g.* photovoltaic devices or photocatalysis), it is very important to know how the optical properties, such as energy band gap, vary with the synthesis method [47].

The ZnO/CdS core–shell materials belong to type-II semiconductors and the optical band gap (E_g) can be estimated using the Tauc relation [48]:

$$\alpha h \nu = C \left(h \nu - E_g \right)^n \tag{1}$$

where α is the absorption coefficient of the CdS at a certain value of wavelength λ, h is Planck's constant, C is the proportionality constant, ν is the frequency of light, and $n = \frac{1}{2}$ (for direct transition mode materials).

The absorption coefficient is evaluated using the relation:

$$\alpha = k \cdot ln \left(\frac{R_{max} - R_{min}}{R - R_{min}} \right) \tag{2}$$

where k is a constant, R_{max} is the maximum reflectance and R_{min} is the minimum reflectance.

The consideration of Eqs. (1) and (2) gives Eq. (3):

$$(\alpha h \nu)^2 = C' \left(h \nu - E_g \right) \tag{3}$$

where C' is a constant. From Eq. (3), a Tauc plot can be drawn of $(\alpha h \nu)^2$ versus $h \nu$. The point of the extrapolation of the linear part that meets the abscissa will give the value of the band gap energy of the material [48, 49].

Fig. 4 shows the Tauc plot for the ZnO/CdS samples. The results may be correlated with structural characteristics, the relationship between band gap and particle dimension, and thus the size effect on the electronic properties of semiconductors, which was previously observed for other materials [50, 51].
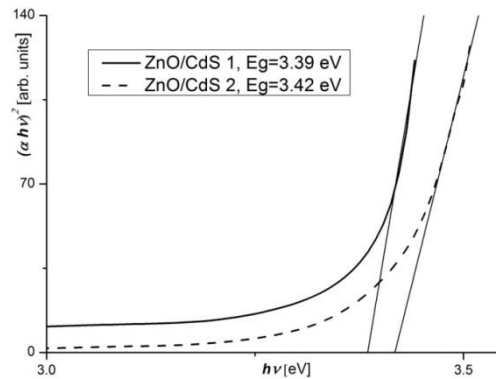
Fig. 4. Tauc plots for ZnO/CdS samples.

The values were compared with those determined for CdS nanopowders obtained in the same conditions, *i.e.* 3.39 eV (for ZnO/CdS **1**) *vs.* 2.67 eV (for PEG-capped CdS [27], estimated by Tauc method) and 3.42 eV (for ZnO/CdS **2**) *vs.* 2.98 eV (for MAA-functionalized CdS [28]); thus, the energy gaps of both ZnO/CdS samples are superior to those of CdS nanopowders.

3.2. Photocatalytic properties

The study of catalytic activity for capped nanoparticles is very interesting, because the capping agents play a versatile role in colloidal synthesis of nanoparticles, different from stabilizers [33].

The catalytic properties of obtained ZnO/CdS powders were demonstrated in the photocatalytic degradation of Congo red solutions. The UV−Vis absorbance spectra indicated the disappearance of CR by breaking up the azo bond, measuring the absorbance at $\lambda = 497$ nm (the azo bond degradation) as a function of irradiation time. The CR concentration was calculated from the absorbance values for the CR solutions and the bleaching of the solutions was estimated by the C_t/C_0 ratio.

The most efficient catalytic activity was observed for ZnO/CdS **1**, the degradation of CR in its presence being faster than for ZnO/CdS **2** powder (Fig. 5). As an overview, the catalytic activity of both samples is slightly dependent on illumination, with a more pronounced dependence for ZnO/CdS **2**. For example, after 120 min, the values for photocatalytic activity are: PA = 74.50% without illumination and PA = 79.86% with illumination (ZnO/CdS **1**); PA = 57.40% without illumination and 64.05% with illumination (ZnO/CdS **2**).
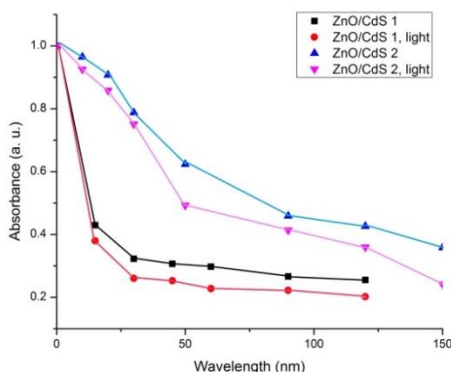
Fig. 5. The photocatalytic degradation curves of CR over the ZnO/CdS powders, in different conditions.

The catalytic activity of ZnO/CdS powders was compared with those of CdS nanopowders obtained in the similar conditions. Thus, the ZnO/CdS **1** powder was compared with PEG-capped CdS nanopowder, obtained in solution [27]; for ZnO/CdS **1** the photocatalytic activity after 90 min was 73.40%, respective 77.77% (light) while for CdS nanopowder obtained in the same conditions, after 100 min, it was 52.89%, respective 59.24% (light). These results demonstrated that the deposition of PEG-capped CdS nanoparticles on the ZnO powder led to an enhanced catalytic activity of CdS nanopowder.

The ZnO/CdS **2** powder was compared with mercaptoacetate functionalized CdS nanopowder [28]; for ZnO/CdS **2** the photocatalytic activity after 90 min was 54.13%, respective 58.67% (light), while for CdS nanopowder obtained in the same conditions it was 20.05%, respective 44.26% (light), demonstrating that the deposition of mercaptoacetate-functionalized CdS nanoparticles on the ZnO powder also caused a catalytic activity improvement compared to CdS nanoparticles. In conclusion, the deposition of the CdS nanoparticles onto ZnO is a convenient technique to improve the catalytic activity of CdS nanopowders [27, 28].

The CR solution is not only bleached in the presence of ZnO/CdS powders, but the dye is decomposed because the intensity of band assigned to aromatic rings in the electronic spectra also decreased in time (Fig. 6).
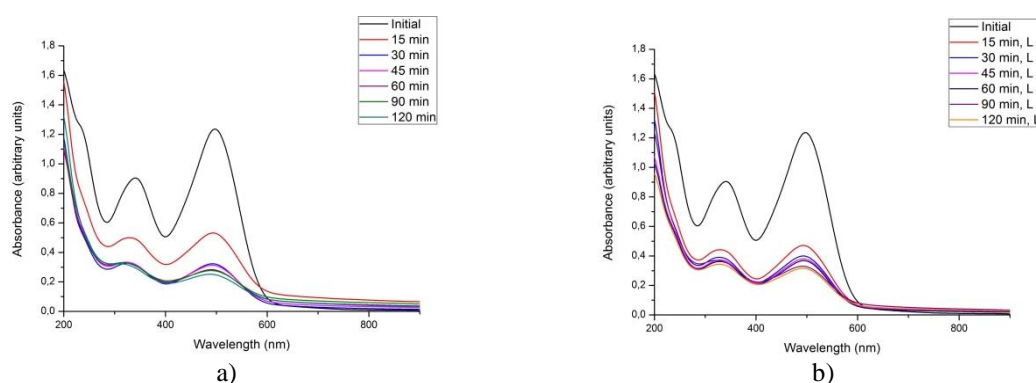
*Fig. 6. The UV–Vis spectral changes of RC solutions as function of time
in ambient conditions (a), respective with illumination (b).*

However, the ratio between the intensity of the bands assigned to azo group, respective to aromatic rings increased in time, a feature which may prove a faster breakdown of azo bond in comparison with the degradation of aromatic rings.

4. Conclusions

The cadmium sulfide is considered to be the most suitable visible sensitizer for zinc oxide, in order to improve its properties by absorbing the visible light and generating the electron–hole pairs; the same, the cadmium sulfide properties can be also enriched by depositing onto zinc oxide surface.

We obtained ZnO/CdS composites powders by the deposition of capped/functionalized CdS nanoparticles onto ZnO surface, using PEG-200 and mercaptoacetate as capping/functionalizing agents. We compared two synthesis techniques, namely the chemical precipitation in aqueous solution and the trituration of non-aqueous mixture. The CdS-decorated ZnO heterostructures have different morphologies, having in view the deposition of CdS nanoparticles onto the ZnO surface. The chemical precipitation in solution led to a more uniform decoration of ZnO with CdS nanoparticles, but the results are also influenced by the presence of functionalization agent; thus, the deposition of functionalized CdS, with an amorphous appearance, onto ZnO particles seems to be less favored, despite the trituration technique provide a close contact between particles during the synthesis in the non-aqueous medium. The absorption bands of these composite materials are broader compared with each semiconductor (CdS and ZnO), their band gap energy values being around 3.40 eV. Different photocatalytic activity of ZnO/CdS samples was determined, both materials exhibiting higher activity compared to the similar CdS nanopowders. Thus, the deposition of CdS nanoparticles onto the ZnO powders resulted on materials with wider band gaps and higher catalytic activity in comparison with CdS nanopowders, being a solution for more environmental friendly materials which can be used as better catalysts.

Acknowledgments

114

References

[1] J. Nayak, Mater. Chem. Phys. **133**, 523 (2012).

[2] Ü. Özgür, Y.I. Alivov, C. Liu, A. Teke, M.A. Reshchikov, S. Doğan, V. Avrutin, S.J. Cho, H. Morkoç, J. Appl. Phys. **98**, 041301 (2005).

[3] H. Yang, C. Huang, X. Li, R. Shi, K. Zhang, Mater. Chem. Phys. **90**, 155 (2005).

[4] H. Lee, H. Yang, P.H. Holloway, Physica B **404**, 4364 (2009).

[5] N.S. Das, P.K. Ghosh, M.K. Mitra, K.K. Chattopadhyay, Physica E **42**, 2097 (2010).

[6] G.A. Martínez-Castañón, J.P. Loyola-Rodríguez, J.F. Reyes-Macías, N. Niño-Martínez Facundo Ruiz, Superficies y Vacío **23**, 1 (2010).

[7] J. Nayak, S.N. Sahu, J. Kasuya, S. Nozaki, Appl. Surf. Sci. **254**, 7215 (2008).

[8] A. Maurya, P. Chauhan. Mater. Charact. **62**, 382 (2011).

[9] L. Wang, H. Wei, Y. Fan, X. Liu, J. Zhan, Nanoscale Res. Lett. **4**, 558 (2009).

[10] T. Tsuzuki, P.G. McCormick, Appl. Phys. A **65**, 607 (1997).

[11] L. Irimpan, V.P.N. Nampoori, P. Radhakrishnan, Sci. Adv. Mater. **2**, 117 (2010).

[12] G. Murugadoss, Particuology **10**, 722 (2012).

[13] J. Nayak, H. Lohani, T.K. Bera, Curr. Appl. Phys. **11**, 93 (2011).

[14] S. Kandula, P. Jeevanandam, J. Nanopart. Res. **16**, 2452 (2014).

[15] X. Wang, G. Liu, L. Wang, Z.G. Chen, G.Q. Lu, H.M. Cheng, Adv. Energy Mater. **2**, 42 (2012).

[16] X. Wang, G. Liu, Z.G. Chen, F. Li, L. Wang, G. Qing Lu, H.M. Cheng, Chem. Commun. **23**, 3452 (2009).

[17] S. Khanchandani, S. Kundu, A. Patra, A.K. Ganguli, J. Phys. Chem. C **116**, 23653 (2012).

[18] C. Li, T. Ahmed, M. Ma, T. Edvinsson, J. Zhu, Appl. Catal. B Environ. **138–139**, 175 (2013).

[19] M. Villani, D. Calestani, L. Lazzarini, L. Zanotti, R. Mosca, A. Zappettini, J. Mater. Chem. **22**, 5694 (2012).

[20] Q. Cui, C. Liu, F. Wu, W. Yue, Z. Qiu, H. Zhang, F. Gao, W. Shen, M. Wang, J. Phys. Chem. C **117**, 5626 (2013).

[21] J.K. Vaishnav, S.S. Arbuj, S.B. Rane, D.P. Amalnerkar, RSC Adv. **4**, 47637 (2014).

[22] U. Shaislamov, H. Kim, B.L. Yang, J. Mater. Res. **28**, 497 (2013).

[23] Q. Yang, Y. Li, Z. Hu, Z. Duan, P. Liang, J. Sun, N. Xu, J. Wu, Optics Express **22**, 8617 (2014).

[24] J. Geng, X.D. Jia, J.J. Zhu, Cryst. Eng. Comm. **13**, 193 (2011).

[25] J. Liu, K. Zhu, B. Sheng, Z. Li, G. Tai, J. Qiu, J. Wang, J. Chen, Y. You, Q. Gu, P. Liu, J. Alloy. Compd. **618**, 67 (2015).

[26] M.H. Habibi, M.H. Rahmati, Spectrochim. Acta A **133**, 13 (2014).

[27] A. Dumbrava, G. Prodan, D. Berger, M. Bica, Powd. Technol. **270**, 197 (2015). doi: 10.1016/j.powtec.2014.10.012

[28] A. Dumbrava, D. Berger, G. Prodan, F. Moscalu, A. Diacon, Mater. Chem. Phys. **173**, 70 (2016). doi:10.1016/j.matchemphys.2016.01.040

[29] L. Ren, Y. Li, J. Hou, X. Zhao, C. Pan, ACS Appl. Mater. Interfaces **6**, 1608 (2014).

[30] T. Leshuk, R. Parviz, P. Everett, H. Krishnakumar, R.A. Varin, F. Gu, ACS Appl. Mater. Interfaces **5**, 1892 (2013).

[31] N. Soltani, E. Saion, W.M.M. Yunus, M. Navasery, G. Bahmanrokh, M. Erfani, M.R. Zare, E. Gharibshahi, Sol. Energy **97**, 147 (2013).

[32] M. Movahedi, A.R. Mahjoub, S. Janitabar-Darzi, J. Iran. Chem. Soc. **6**, 570 (2009).

[33] Z. Niu, Y. Li, Chem. Mater. **26**, 72 (2014).

[34] O. Estévez-Hernández, J. González, J. Guzmán, P. Santiago-Jacinto, L. Rendón, E. Montes, E. Reguera, Sci. Adv. Mater. **4**, 771 (2012).

[35] Y. Abe, A. Komatsu, H. Nohira, K. Nakanishi, T. Minemoto, T. Ohta, H. Takakura, Appl. Surf. Sci. **258**, 8090 (2012).

[36] T. Tanigaki, S. Kimura, N. Tamura, C. Kaito, Jpn. J. Appl. Phys. **41**, 5529 (2002).

[37] A. Dumbrava, G. Prodan, F. Moscalu, Mat. Sci. Semicon. Proc. **16**, 1095 (2013). doi: 10.1016/j.mssp.2013.03.007

[38] S. Musić, A. Šarić, S. Popović, J. Alloys Compd. **429**, 242 (2007).

[39] S. Musić, A. Šarić, S. Popović, J. Alloys Compd. **448**, 277 (2008).

[40] J. Coates, Interpretation of Infrared Spectra. A Practical Approach, in Encyclopedia of Analytical Chemistry. R. A. Meyers (Ed.), John Wiley & Sons, Chichester, **2000**, pp.10815–10837.

[41] A. Kharazmi, N. Faraji, R.M. Hussin, E. Saion, W.M.M. Yunus, K. Behzad, Beilstein J. Nanotechnol. **6**, 529 (2015).

[42] M. Koneswaran, R. Narayanaswamy, Sensor Actuat. B Chem. **139**, 91 (2009).

[43] C. Chung, M. Lee, Bull. Korean Chem. Soc. **25**, 1461 (2004).

[44] E. Pretsch, P. Bühlmann, M. Badertscher, Structure Determination of Organic Compounds, fourth edition, Springer-Verlag Berlin Heidelberg, **2009**, pp. 289, pp. 314-315.

[45] F. Chen, Y. Cao, D. Jian, X. Niu, Ceram. Int. **39**, 1511 (2013).

[46] W. Xu, Y. Wang, R. Xu, S. Liang, G. Zhang, D. Yin, J. Mater. Sci. **42**, 6942 (2007).

[47] N.S. Das, P.K. Ghosh, M.K. Mitra, K.K. Chattopadhyay, Physica E **42**, 2097 (2010).

[48] J. Tauc, R. Grigorovici, A. Vancu, Phys. Status Solidi B **15**, 627 (1966).

[49] R. Rusdi, A.A. Rahman, N.S. Mohamed, N. Kamarudin, N. Kamarulzaman, Powd. Techn. **210**, 18 (2011).

[50] P.E. Lippens, M. Lannoo, Physical Rev. B **39**, 10935 (1989).

[51] A. Dumbrava, G. Prodan, A. Georgescu, F. Moscalu, Bull. Mater. Sci. **38**, 1 (2015). dx.doi.org/10.1007/s12034-014-0793-8